IEEE Access
Multidisciplinary | Rapid Review | Open Access Journal

Received August 11, 2020, accepted August 20, 2020, date of publication August 26, 2020, date of current version September 9, 2020.

Digital Object Identifier 10.1109/ACCESS.2020.3019663

Compacted Conformal Implantable Antenna With Multitasking Capabilities for Ingestible Capsule Endoscope

MUHAMMAD YOUSAF[1], ISMAIL BEN MABROUK[2], (Senior Member, IEEE), FAROOQ FAISAL[3], MUHAMMAD ZADA[4], ZUBAIR BASHIR[1], ADEEL AKRAM[1], MOURAD NEDIL[3], (Senior Member, IEEE), AND HYOUNGSUK YOO[4], (Senior Member, IEEE)

[1]ACTSENA Research Group, Telecommunication Engineering Department, University of Engineering and Technology Taxila, Taxila 47050, Pakistan
[2]Department of Electrical Engineering, Al Ain University of Science and Technology, Abu Dhabi, United Arab Emirates
[3]Department of Electrical Engineering, University of Quebec, Val d'Or, QC J9P 1S2, Canada
[4]Department of Biomedical Engineering, Hanyang University, Seoul 04763, South Korea

Corresponding authors: Ismail Ben Mabrouk (ismail.mabrouk@aau.ac.ae) and Hyoungsuk Yoo (hsyoo@hanyang.ac.kr)

This work was supported in part by the Basic Science Research Program through the National Research Foundation of Korea funded by the Ministry of Education, Science and Technology under Grant 2019R1A2C2004774, and in part by the ADEK Award for Research Excellence (AARE) 2018.

ABSTRACT This study presents a multi-band conformal antenna based endoscopic system for robust biotelemetry communications, which covers five important bands, including the MedRadio (401–406 MHz), Industrial, Scientific, and Medical (ISM) (433.1–434.8 MHz, 868–868.6 MHz, 902–928 MHz), and midfield (1200 MHz) bands. These bands are intended for functions such as biotelemetry, power saving, and wireless power transfer (WPT). The proposed antenna is printed on a flexible material Rogers ULTRALAM with a thickness of only 0.1 mm, which can be easily wrapped around the inner wall of a capsule. Owing to the insertion of the via and open-ended meandered slots in the radiator and in the ground plane, the footprints of the suggested antenna reduce considerably. In the flat form, the antenna is 57 mm^3 in volume, whereas in the wrapped form, it is only 48.98 mm^3 in volume. In a homogeneous muscle phantom, the proposed conformal antenna shows a 27.46% wider bandwidth at 402 MHz,whereas it shows a 13.2% and 5.42% bandwidth at 915 MHz and 1200 MHz, respectively. Furthermore, the specific absorption rate investigation at three resonance frequencies in various implanted locations shows compliance with the IEEE guidelines, thereby guaranteeing human safety. For measurements, a 3D capsule with batteries and circuitry is devised using a 3D printer, and the simulation results are experimentally validated in a box containing minced pork. Finally, the robustness of the communication link is confirmed through the link budget analysis at 1 Mb/s. The conformal design concept, omni-directional radiations, and multi-band functionality with a wider bandwidth in the MedRadio band of the suggested antenna will enhance the diversity of the capsule endoscope and be a good addition to the field of biotelemetry.

INDEX TERMS Biotelemetry, conformal antenna, link budget, multi-band, specific absorption rate.

I. INTRODUCTION

Wireless capsule endoscopy (WCE) is a noninvasive method used to record and deliver images of the gastrointestinal (GI) tract for medical analysis [1]. The WCE can examine regions of the GI tract, which cannot be accessed using the traditional wired endoscope. The antenna employed in WCE is responsible for the radiation and reception of the electromagnetic (EM) waves, thereby enabling establishment of a communication link between the external equipment and the capsule. The establishment of a robust wireless link between an endoscopic antenna and an external station is challenging owing to various factors [2]. Recent studies on capsule/endoscopic antennas have shown that conformal [3] and embedded structures [4] are the preferred types of antennas. The embedded-type antennas are set inside the

The associate editor coordinating the review of this manuscript and approving it for publication was Nuno Garcia.

endoscope cavity; however, they exhibit lower radiation efficiency when compared to the conformal antennas. On the contrary, the conformal antennas use only the outer or inner surface of the capsule, thereby allowing the interior to be utilized by the batteries and related circuitry. This allows an antenna of a larger size to be used for better performance and makes the most effective use of the available capsule surface area [5].

Several frequency bands are allocated for biomedical applications. Most of the commercially available IWMDs (endoscopes) operate in the MedRadio frequency band (401–406 MHz). The higher license free ISM bands (0.915 GHz, 2.45 GHz, and 5.8 GHz) are preferred for applications requiring high data rates. However, at 2.45 GHz and 5.8 GHz, the losses become dominant owing to the increase in the tissues conductivity with increase in frequency. Moreover, these bands are overloaded due to its use by Bluetooth, WLAN, ZigBee, and other modern wireless systems, thus causing considerable interference. Additionally, the telemetry range decreases due to increase in path-loss at higher frequency bands. Consequently, a suitable frequency band combining lower SAR, small size, and reduced interference along with an adequate bandwidth, is essential. Therefore, the 402 MHz MedRadio, 434 MHz, 868 MHz, and 915 MHz ISM, and 1200 MHz midfield bands were targeted in this study.

A two-layered single-band circular polarized (CP) implantable antenna 15 mm × 15 mm × 1.27 mm in size was proposed in [6]. Despite the superstrate and substrate rigidity, a narrow simulated bandwidth of 97 MHz was achieved in a cubic phantom assigned with electric properties of human skin at 0.915 GHz. In [7], a multi-layered helical antenna operating at 2.4 GHz was reported for endoscopy. However, this helical implantable antenna has a small gain of −32 dBi and a complex geometry with a bulky volume of 302.05 mm^3. The single-band antennas may not meet all the requirements of an implanted wireless medical device (IWMD) because these devices require operating frequencies for functionalities such as wireless charging and waking-up along with biotelemetry [8]. Consequently, there has been an increased demand for multiband ingestible antennas.

In literature, only a few ingestible implantable antennas with dual- and triple-band operations have been proposed [9]–[12]. Hence, the potentials of multi-band ingestible antennas have not yet been completely exploited. In [9], we reported a dual-band antenna with flower-shaped radiator for skin implantations and endoscopy applications. Besides the drawbacks regarding structural complexity and a small gain at 2.45 GHz, the study lacked a system-level analysis. Similarly, the two dual-band antennas proposed in [10] and [11] may not comply with most IWMDs owing to the lack of frequencies for power saving or wireless power transfer (WPT).The tri-band implantable antenna [12] operating at 0.915 GHz and 2.45 GHz industrial, scientific, and medical (ISM) bands, and 1.9 GHz midfield band was designed on a rigid substrate for deep tissues and skin implantation. However, the simulated bandwidths obtained in these three bands were very small (8.7%, 7.3%, and 8.2% at 0.915 GHz, 1.9 GHz, and 2.45 GHz, respectively) and therefore increased the possibility of detuning threats in a practical scenario. In [13], a dual CP antenna having a conformal structure and wide bandwidth characteristics was proposed. The antenna was integrated with an endoscopic capsule and the wireless link was characterized through simulations and experiments. However, the antenna suffers feed complexity due to the loop structure, thus not possible to feed the antenna in the flat condition.

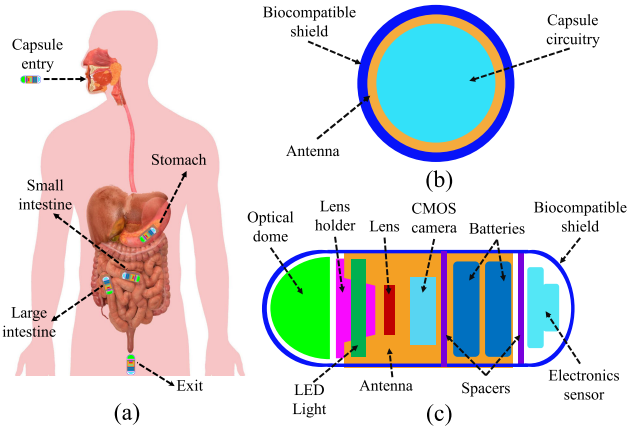

FIGURE 1. (a) Wireless capsule endoscopy. (b) Cross-sectional view of the designed capsule endoscope. (c) Side view of the designed capsule endoscope.

In this study, a multi-band conformal implantable antenna integrated with a capsule system covering the MedRadio, midfield, and three ISM bands is presented for multi-tasking. The structure of the capsule endoscope 11 mm × 26 mm in dimension and containing an optical dome, batteries, a camera, LEDs, sensors, and an antenna is displayed in Fig. 1. Owing to the multi-band operation with a wide bandwidth in the MedRadio band, the proposed antenna system can perform data telemetry, power saving, and WPT simultaneously. Table 1 shows a detailed performance-based comparison of the proposed multi-band conformal antenna with some recent research on implantable antennas. It can be observed that the proposed conformal antenna exhibits prominent properties regardless of its flexible structure and multi-band functionality with wideband characteristics in the MedRadio band. Initially, the antenna was simulated individually at the center of a homogeneous muscle phantom (HMP) in its flat and conformal forms. It was then integrated with a capsule device containing batteries and related circuitry, and its performance was analyzed by conducting simulations in the same HMP. Detuning caused by the components of the device was overcome via updating of the width of the antenna ground slots. Subsequently, the results of the device obtained in the HMP were verified in the stomach, small intestine, and large intestine of a heterogeneous human model. To ensure

TABLE 1. Performance comparison of proposed multi-band conformal antenna with recent research.

Ref.	Year	Frequency (MHz)	Volume (mm^3)	Bandwidth (%age)	Gain (dBi)	SAR (W/kg)		Antenna type
						1-g	10-g	
[1]	2018	433	104.5	112.5	-35	--	--	Conformal
[2]	2018	2450	116.5	--	-24.14	217.2	--	Conformal
[3]	2017	434	9	4	-22.4	--	--	Conformal
[4]	2011	500	392.7	20.9	-19.9	--	--	Embedded
[6]	2017	915	285.8	10.6	-27	517	--	Embedded
[7]	2014	2450	362	40	-34.6	126	26.8	Embedded
[8]	2017	402 915 2450	106	11.3 9.14 19.8	-29.7 -24.9 -23.2	216.6 92.4 98.5	--	Conformal
[11]	2018	915 2450	24	9.84 8.57	-28.5 -22.8	971.6 807.3	118.3 102	Embedded
[12]	2018	915 1900 2450	21	8.7 8.2 7.3	-26.4 -23 -20.5	380 358 363	40.4 38.2 40.3	Embedded
[14]	2016	405 915 2450	52.5	15.8 10.1 4.3	-40.85 -32.98 -22.37	665.4 837.7 759.7	93.24 93.97 87.24	Embedded
This work	2020	402 915 1200	48.98	38.6 19.6 8.1	-30.8 -19.7 -18.7	289.0 263.5 214.9	60.9 53.9 50.5	Conformal

user safety, the specific absorption rate (SAR) analysis of the entire system was also conducted in the three different aforementioned heterogeneous implanted organs. Furthermore, the wireless link viability was confirmed via the link budget analysis. The simulation results achieved in different scenarios were validated via measurement of the fabricated 3D capsule in the minced pork phantom.

II. DESIGN METHODOLOGY

This study aims to design a multi-band compact conformal antenna for capsule endoscopy, which can efficiently perform simultaneous biotelemetry, WPT, and power saving. The detailed geometry of the proposed conformal antenna with dimensions of 19 mm × 15 mm × 0.2 mm is displayed in Fig. 2. The geometric values shown in Fig. 2 were obtained inside an HMP. As shown in Figs. 2(a) and (b), the meandered shaped slots with open ends were created in the antenna radiator and ground. These slots, along with the shorting pin, were responsible for a considerable reduction in size, tuning to the desired frequencies, and bandwidth enhancement of the proposed antenna. The radiator of the designed conformal antenna is backed by a biocompatible and flexible Rogers ULTRALAM substrate [dielectric constant $(\varepsilon_r) = 2.9$ and tangent loss $(\tan\delta) = 0.0025$] with a thickness of 0.1 mm [15]. For the superstrate, a layer of a bio-plastic material polylactic acid (PLA) with a thickness = 0.1 mm, $\varepsilon_r = 3.1094$, and $\tan\delta = 0.0053$ was laid over the proposed antenna, which was the same material used for the capsule shell. Before the antenna was integrated with the capsule, the superstrate layer was removed. The primary function of the PLA superstrate in the flat form of the proposed antenna was to avoid its mismatching following integration into the capsule. However, it also helped in size reduction as investigated in [16]. For excitation of the antenna, a coaxial feed of 50 Ω and a radius of 0.2 mm was used. The multi-band functionality with satisfactory bandwidths was achieved through the open-ended slots and moving the feed and via to the most suitable positions. Table 2 presents all the parameters of the proposed conformal antenna.

A. CONSIDERED SIMULATION AND MEASUREMENT SCENARIOS

The design of the proposed conformal antenna-based endoscopic system was created and simulated using the finite element method (FEM)-based simulator Ansoft HFSS and the finite difference time domain (FDTD)-based Remcom

TABLE 2. Antenna parameters before and after optimization.

Variable	Value (mm)		Variable	Value (mm)	
	Before optimization	After optimization		Before optimization	After optimization
W_a	19.0	19.0	L_2	10.0	10.0
W_1	1.4	1.4	L_3	12.0	12.0
W_2	0.8	0.8	L_4	0.8	0.8
W_3	0.6	0.6	L_5	7.5	7.5
W_4	2.2	2.2	L_6	3.2	3.2
W_5	0.7	0.7	L_7	0.8	0.8
W_6	0.8	0.8	L_8	2.6	2.6
W_7	11.9	11.9	L_9	6.6	6.6
W_8	10.6	10.6	L_{10}	0.5	0.5
W_9	7.15	7.15	L_{11}	8.2	8.2
W_{10}	7.2	7.2	L_{12}	0.7	0.7
W_{11}	9.9	9.9	L_{13}	3.5	3.5
W_{12}	13.5	13.5	L_{14}	2.1	2.1
W_{13}	2.1	2.1	L_{15}	1.0	1.3
W_{14}	9.5	9.5	L_{16}	13.5	13.5
W_{15}	5.0	5.0	L_{17}	1.0	1.0
W_{16}	0.8	0.4	L_{18}	1.5	1.5
W_{17}	5.2	5.2	L_{19}	6.0	6.0
W_{18}	1.0	1.0	f_x	10.8	10.8
W_{19}	5.0	5.0	f_y	2.5	2.5
L_a	15.0	15.0	S_x	0.7	0.7
L_1	13.6	13.6	S_y	3.0	3.0

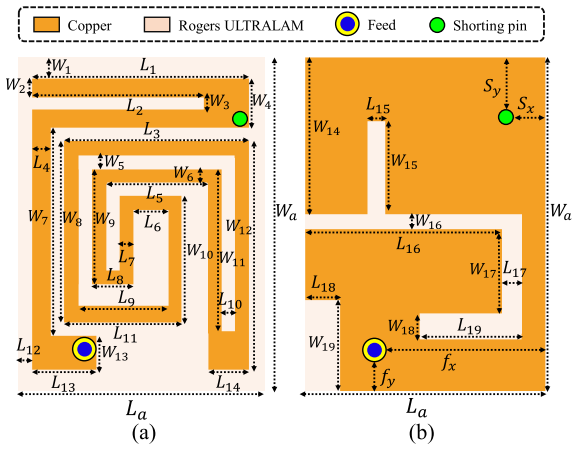

FIGURE 2. Geometry of suggested multi-band conformal antenna. (a) Front view. (b) Rear view.

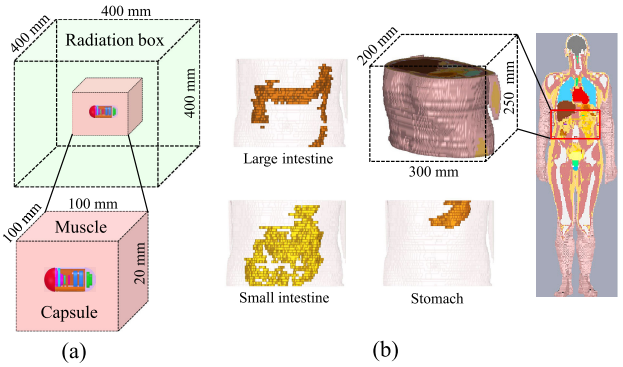

FIGURE 3. Simulation scenarios. (a) Homogeneous. (b) Heterogeneous.

and CST simulators. Primarily, the antenna was individually kept flat and conformal at the center of the HMP with dimensions of 20 mm × 100 mm × 100 mm in HFSS, as depicted in Fig. 3(a). Next, it was integrated with an endoscopic capsule, and the same HMP was used for the further analysis. To validate the performance in a more real approaching scenario, the proposed system was implanted in the stomach, small intestine, and large intestine of a realistic heterogeneous model in the FDTD-based simulator, as illustrated in Fig. 3(b). The permittivity and conductivity properties of the HMP and aforementioned organs at three achieved resonance frequencies are shown in Table 3. The prototypes of the multi-band conformal antenna and the 3D capsule along with the corresponding circuitry were fabricated, as shown in Figs. 4(a) and (b), respectively. The measurement setups, shown in Figs. 4(c) and (d), were used for the simulated S_{11} and radiation patterns validation, respectively.

TABLE 3. Properties of human tissues at various frequencies.

Phantom	Relative permittivity (ε_r)			Conductivity (σ) (S/m)		
	Frequency			Frequency		
	402 MHz	915 MHz	1200 MHz	402 MHz	915 MHz	1200 MHz
Muscle	57.1	55.0	54.4	0.797	0.948	1.06
Large intestine	62.6	57.9	56.7	0.859	1.09	1.23
Stomach	67.5	65.0	64.3	1.00	1.19	1.33
Small intestine	66.1	59.4	57.9	1.90	2.17	2.33

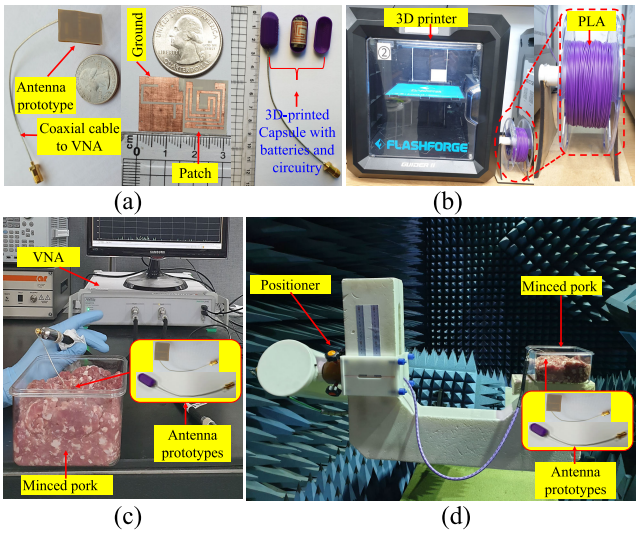

FIGURE 4. (a) Conformal antenna fabricated prototypes. (b) 3D-printed capsule with batteries and related circuitry. (c) S_{11} measurement setup. (d) Radiation patterns measurement setup.

B. MULTI-BAND ANTENNA DESIGN EVOLUTION

As illustrated in Fig. 5(a), the proposed conformal multi-band antenna with wideband characteristics in the band of 402 MHz was designed and evolved via four successive steps. It is evident that the final multi-band design was obtained via conduction of step-wise modifications in a simple rectangular patch antenna. These modifications were made in the form of the insertion of a shorting-pin and removal of strips from the patch and ground plane to achieve better performance parameters and antenna miniaturization. It is noteworthy to mention that the dimensions of all the cuts were selected after a comprehensive parametric study based on reflection coefficient (S_{11}). It can be observed from Fig. 5(b) that antenna S_{11} improves owing to the step-wise modifications in its design.

C. CURRENT DISTRIBUTIONS

Figs. 6(a)–(c) show the surface currents on the radiator and ground plane at 402 MHz, 915 MHz, and 1200 MHz before the antenna was wrapped. It can be observed that at 402 MHz, the currents on the ground plane (Fig. 6(a)) generated near the port, flow towards the shorting pin where they couple with the ground plane. Whereas, the current on

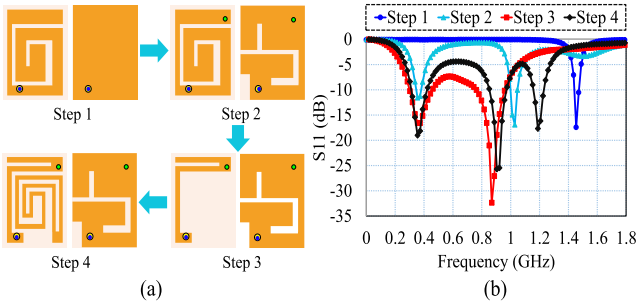

FIGURE 5. (a) Designing steps. (b) S_{11} of the corresponding designing steps.

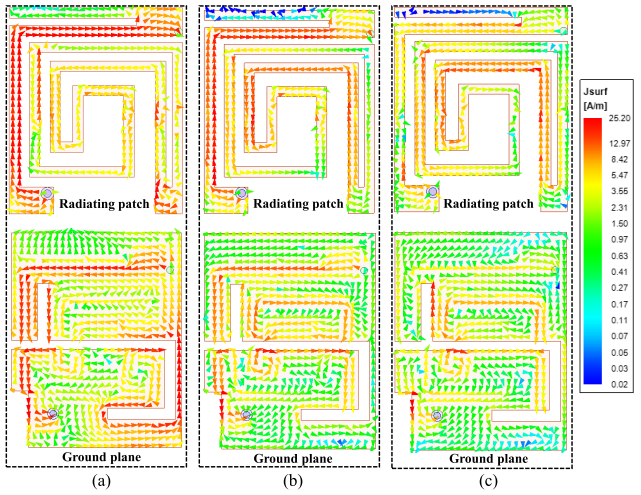

FIGURE 6. Current distributions. (a) 402 MHz. (b) 915 MHz. (c) 1200 MHz.

the ground plane following a much longer path to constitute 402 MHz band. Here, the currents on the main radiator flow unidirectionally, following the quarter wavelength monopole mode [21]. The currents at 915 MHz (Fig. 6(b)) also show the same behavior on the main radiator as those at 402 MHz. However, the current intensities are much lower than those at 402 MHz. In other words, the electrical length of the antenna decreased compared to the lower resonance mode. Moreover, the currents on the parasitic patch became smoother and more balanced resulting in impedance matching at 915 MHz. Fig. 6(c) shows the surface currents at 1200 MHz. It can be seen that the currents on the main radiating patch are changing their directions while flowing towards the port, following the half wavelength monopole mode [8]. The electrical length of the antenna at the higher frequency band was decreased because the currents take much shorter paths to flow on the radiator as well as on the ground plane compared to the other lower resonance modes. Additionally, it can be clearly seen that at 402 MHz and 915 MHz, majority of the currents on the main radiating patch and in adjacent sections of the parasitic element are flowing in opposite directions. It shows that the passive elements is not resonating at these two lower frequencies. However, at 1200 MHz, the currents on the mentioned parts of the resonator become parallel to each other. It clearly shows that the parasitic element is contributing in the resonance at 1200 MHz. It is noteworthy

that the current intensities around the ground slots at the desired frequencies are higher compared to those around the radiating patch. These higher current densities can detune the operating frequencies of the antenna owing to the availability of capsule components and batteries that can couple with back radiation from the ground slots. However, the detuning was retuned by updating the ground slot dimensions. Thus, it can be concluded that the ground slots are crucial for tuning owing to the existence of strong currents on its edges.

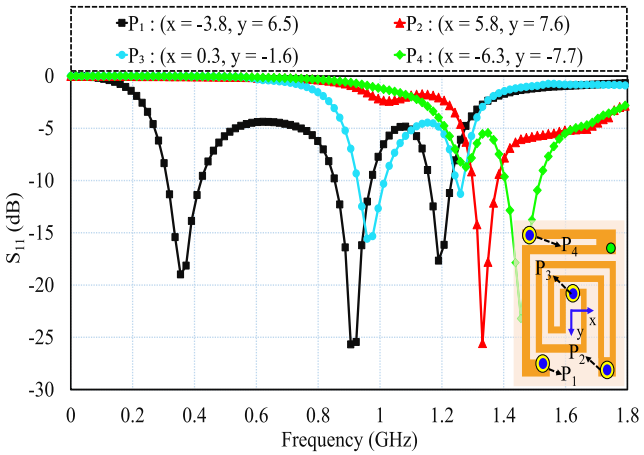

FIGURE 7. Effects on S_{11} due to variations in feed position.

D. EFFECTS DUE TO VARIATIONS IN FEED POSITION

The effects on S_{11} of the proposed antenna owing to the variations in the feed position are shown in Fig. 7. It can be seen that the feed position is crucial to obtain multi-bands for the proposed antenna. Feeding the antenna at P_2 produces a single resonance at 1.33 GHz of 80 MHz narrow bandwidth. However, when the antenna is excited at P_3, two weak resonance modes appear at approximately 970 MHz and 1.26 GHz, thus demonstrating the dual-band behavior of the antenna. Similarly, keeping the feed at P_4 generates a single sharp resonance at 1.46 GHz. It is observed that when the feed and shorting-pin are placed near to each other, the frequency shift to the higher spectrum. It is due to the fact that the current path from the port to the shorting-pin as well as the returning path through a shorting-pin and ground becomes shorter. Moreover, exciting the passive element at various positions control the higher band (1200 MHz). Approaching the feeding point on passive structure near to the adjacent arm of the main radiator, the higher band shifts down to 1200 MHz. From this analysis, we determined that P_1 was the most suitable feed position at which to obtain the multi-band functionality with satisfactory bandwidths in the operating bands.

E. EFFECTS DUE TO VARIATIONS IN VIA POSITION

The effects on S_{11} of the proposed antenna owing to the variations in the via position are displayed in Fig. 8. It can be clearly observed that the via position not only affects the

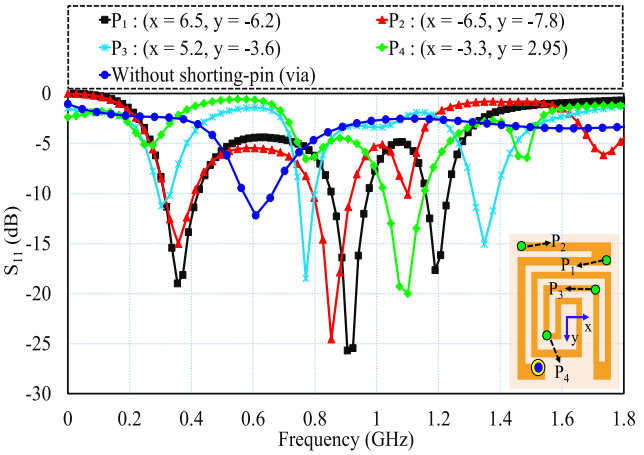

FIGURE 8. Effects on S_{11} due to variations in via position.

antenna impedance matching but also plays an important role in the tuning and achievement of the multi-band functionality. Upon moving the via to P_2, the depths of the first and last resonances decrease, and a shift towards the left side can be observed in all the operating frequencies. When the via is inserted at P_3, a large shift in the upper resonance mode towards the higher frequencies and a significant reduction in the two lower resonance frequencies can be observed. When keeping the via at P_4, the antenna produces only one resonance at approximately 1.1 GHz with a bandwidth of 130 MHz. Finally, the proposed conformal antenna becomes a dual-band operating antenna at 610 MHz and 2.3 GHz when the via is removed. Hence, it can be concluded that in the proposed conformal antenna, the via plays a vital role in the impedance matching, tuning, and achievement of multiple resonances.

F. COUPLING EFFECTS DUE TO ANTENNA INTEGRATION WITH CAPSULE

Thus far, the conformal antenna without capsule/endoscope has been conceived. Nevertheless, in a real scenario, the antenna will be encapsulated with batteries and circuitry, as displayed in Fig. 1. Thus, it is essential to check for coupling issues between the capsule components and the suggested antenna. To execute this, most of the components shown in Fig. 1, such as the lens holder, spacers, CMOS camera, and electronics sensor, were supposed as dielectrics. The perfect electric conductor (PEC) was selected as a material for batteries. For the coupling analysis, the entire system was set at the center of the same HMP, as portrayed in Fig. 3(a). As discussed earlier, strong currents were present around the ground slots edges at three resonance frequencies (Fig. 6). Consequently, following integration with capsule, the conformal antenna was detuned from its desired frequencies, which was then retuned via updating of the dimensions of its ground slots(W_{16} and L_{15}), as illustrated in Fig. 9. Subsequently, the results obtained after the retuning of the antenna were validated in the stomach, small intestine,

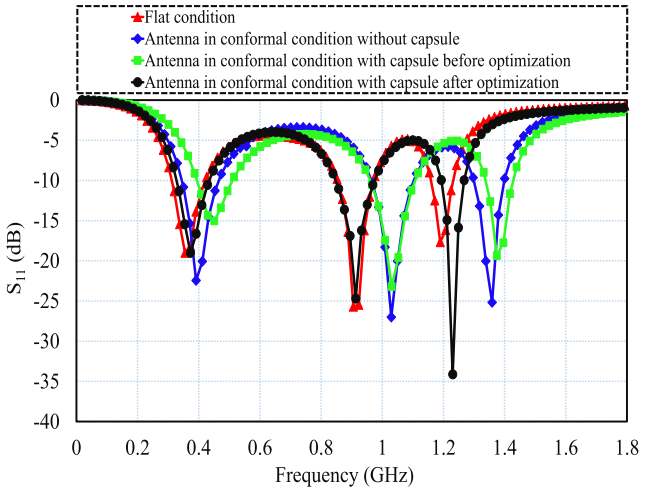

FIGURE 9. Effects on S_{11} due to the coupling of conformal antenna with capsule components.

and large intestine of a heterogeneous human model in the FDTD environment. The drastic changes in the S_{11} at 402 MHz and 1200 MHz due to antenna integration with capsule may be imputed to the alteration in the antenna impedance matching at these frequencies. The geometrical values of the ground slots before and after retuning are shown in Table 2.

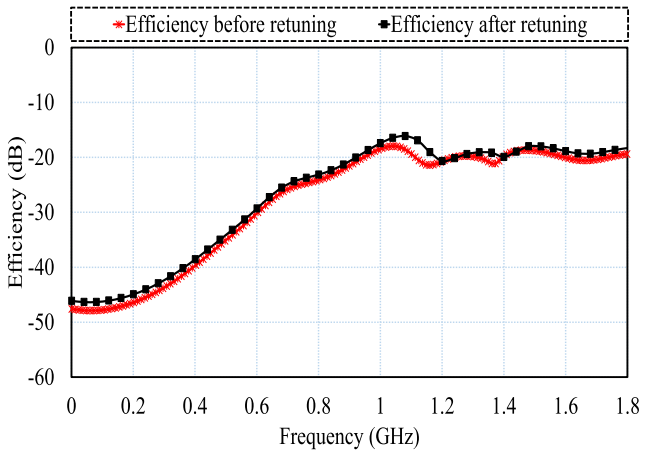

FIGURE 10. Efficiency of the conformal antenna before and after retuning.

G. ANTENNA EFFICIENCY BEFORE AND AFTER RETUNING

Fig. 10 displays the efficiency values of the conformal antenna over all the achieved resonances before and after retuning. The efficiency of antennas after implantation in the human tissues drastically decreases due to the strong coupling with the tissues and absorption of radiations. Depending on the implantation depth and tissue type, implantable antennas usually have an efficiency of less than or equal to 1%. As can be seen in both cases of Fig. 10, the total efficiency is greater than −40 dB at all the three resonance frequencies. It can be also observed that the antenna efficiency has increased after its retuning. This increment is due to the improved impedance matching after antenna optimization.

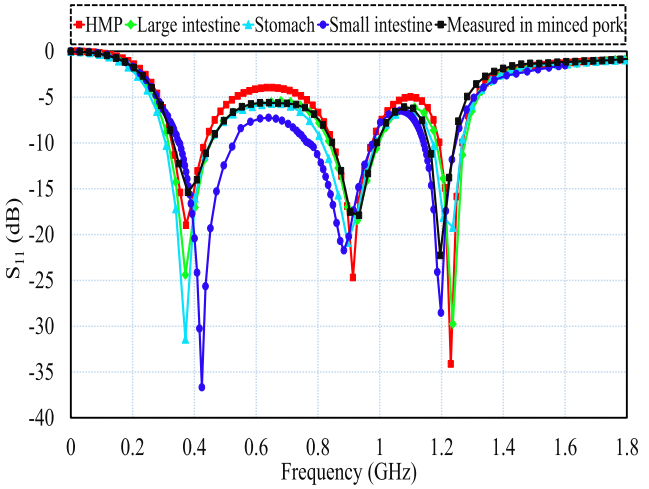

FIGURE 11. S_{11} comparison in different implantation scenarios.

III. RESULTS AND DISCUSSION

To reduce the analysis time, the design of the proposed conformal antenna was initiated and analyzed at the center of an HMP (Fig. 3(a)) in an HFSS simulator. Owing to the diversity in the human tissues, the antenna sensitivity was considered. According to the target application, the proposed conformal antenna-based system was implanted in the stomach, small intestine, and large intestine of a heterogeneous human model in an FDTD based simulator, as shown in Fig. 3(b). To confirm the validity of the simulation results, the fabricated conformal antenna-based 3D capsule was measured in minced pork, as demonstrated in Figs. 4(c) and (d). The comparison S_{11} in the HMP, realistic heterogeneous scenarios, and measured environment is displayed in Fig. 11. It is apparent that the proposed conformal antenna system resonates at 0.402 GHz, 0.915 GHz, and 1.2 GHz with measured bandwidths in the minced pork of 120 MHz, 144 MHz, and 63 MHz, respectively. These bandwidths could encompass five important frequency bands: MedRadio (401–406 MHz), ISM (433.1–434.8 MHz, 868–868.6 MHz, and 902–928 MHz), and midfield (1200 MHz). In Fig. 11, a certain degree of detuning can be observed at three resonance frequencies owing to heterogeneous environments. The greatest shift was recorded in the highly conductive environment of the small intestine, whereas the smallest shift was observed in the large intestine. These shifts in the desired operating bands may be the result of the electrical properties variations [17] and asymmetrical load effects [18] of the heterogeneous tissues. Nevertheless, regardless of the above shifts, the achieved bandwidths still adequately covered all the target frequency bands in all the implanted scenarios.

Fig. 12 shows the far-field polar gain patterns obtained in various simulation scenarios and measured in the minced pork using the setup shown in Fig. 4(d). Among the various implantation scenarios, the lowest gain values (−36.2 dBi,

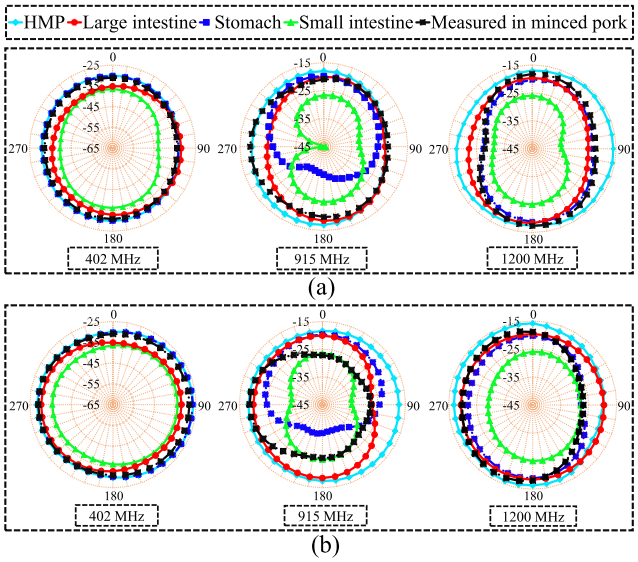

FIGURE 12. Radiation patterns comparison in different implantation scenarios. (a) E-plane. (b) H-plane.

TABLE 4. Summary of antenna performance parameters in different scenarios.

Implanted scenario	Frequency (MHz)	Bandwidth (MHz)	Gain (dBi)	SAR		Max. allowed input power (mW)	
				1-g	10-g	1-g SAR limit	10-g SAR limit
HMP	402	109	-29.8	-	-	-	-
	915	126	-16.9	-	-	-	-
	1200	70	-15.8	-	-	-	-
Large Intestine	402	129	-30.3	277.5	60.3	5.8	33.16
	915	151	-18.4	227.5	49.7	7.03	40.24
	1200	88	-18.3	206.1	44.6	7.8	44.84
Stomach	402	138	-30.8	289.0	60.9	5.53	32.84
	915	166	-19.7	263.5	53.9	6.07	37.10
	1200	93	-18.7	214.9	50.5	7.44	39.60
Small intestine	402	175	-36.2	293.7	64.2	5.44	31.15
	915	206	-25.1	266.6	57.2	6.0	35
	1200	104	-24.9	220.5	51.9	7.25	38.53
Measured	402	120	-30.9	-	-	-	-
	915	144	-18.7	-	-	-	-
	1200	63	-17.3	-	-	-	-

−25.1 dBi, and −24.9 dBi at 402 MHz, 915 MHz, and 1200 MHz, respectively) are observed in the small intestine, whereas the highest values are observed in the HMP, as mentioned in Table 4. The lower gain values in the small intestine are due to its high conductive nature (Table 3) compared to other tissues at all frequency bands. Furthermore, it can be seen in Fig. 12 that in most scenarios, the radiation patterns are nearly omni-directional, like obtained in previous studies [19], [20], which is an essential feature required owing to the changing orientations of the endoscope in the GI tract.

Furthermore, we investigated the safety performance of the proposed capsule endoscopic antenna in the stomach, small, and large intestines based on the IEEE safety regulations. These guidelines restricted the SAR such that 1.6 W/kg and 2 W/kg for 1 g and 10 g of tissues, respectively, were not exceeded. In this safety analysis, we considered 1 W of input power for our proposed endoscopic antenna. Based on this, the calculated values of SAR and the maximum allowed power for the proposed conformal antenna in the stomach, small, and large intestines are shown in Table 4. The higher values of SAR of 293.7 W/kg and 64.2 W/kg are observed in the small intestine for 1 g and 10 g of tissues, respectively. These higher values of SAR were observed owing to the lossy nature of the small intestine at microwave frequencies. However, the calculated maximum allowed power (Table 4) is higher than the specified power of 25 μW [15] for implantable devices. Therefore, the proposed endoscopic antenna is proven safe under the IEEE safety guidelines. The overall performance of the proposed antenna system is summarized in Table 4.

IV. LINK BUDGET ANALYSIS

A biomedical telemetric link allows for the physiological measurements remotely through implantable transducers. Therefore, a reliable communication link is essential between the in-body device and external controlling and/or monitoring device (worn by the patient). However, ensuring the robustness of the communication link is challenging owing to several types of losses such as path loss, reflection, absorption [12], and polarization mismatch losses [11]. In this link analysis, we considered the maximum value for polarization losses to be due to the use of a linear polarized antenna that can change its orientation while it travels through the GI tract. Additionally, to avoid safety issues and interference with nearby devices operating at the same frequencies, the input power and effective isotropic radiated power (EIRP) are restricted for implantable devices. Therefore, the EIRP must be less than or equal to the $EIRP_{max}$ = −16 dBm and 36 dBm for 402 MHz and 915 MHz bands, respectively. At lower frequencies, the signal propagates more reliably in the body when compared to the higher frequencies. Thus, the lower frequencies are more suitable for GI applications and deep skin implantations. In contrast to EIRPs restrictions, the electronic circuits and batteries in the endoscopic device can impose more power restrictions [9]. In the endoscopic capsule-type devices, silver oxide batteries of 20 mW power are used, which can supply 3V at 55 mAh continuously to the circuit for 8–10 hours. Considering these challenges, the transmitter power (P_t) is maintained at −4 dBm, which is lower than the maximum allowed input power (calculated based on the maximum SAR values). The value of B_r is considered to be 1 Mb/s because capsule endoscopy requires a high data rate for transfer of high-quality images to the external base station. To establish a stable communication link between the endoscopic antenna and external device, the antenna power (A_p) should be higher than the required power (R_p). The values of A_p and R_p can be

determined as follows:

$$A_p(dB) = P_{Tx} + G_{Tx} + G_{Rx} - L_f - P_L, \quad (1)$$

$$R_P(dB) = \frac{E_b}{N_o} + KT_o + B_r, \quad (2)$$

where P_{Tx}, G_{Tx}, and G_{Rx} denote the transmitter power, gain of the transmitter, and gain of the receiver antenna, respectively. Depending on the implantation scenario, the value of G_{Tx} is varied according to Table 4, while that of the G_{Rx} is considered to be constant (2 dBi). L_f and P_L denote the free space and polarization mismatch losses, respectively. L_f generally depends on the distance (d) between the transmitter and the receiver. This loss can be computed using the following equations:

$$L_f(dB) = 20log(\frac{4\pi d}{\lambda}). \quad (3)$$

E_b/N_0, K, T_0, and B_r in equation (2) represent the ideal phase shift keying, Boltzmann constant, temperature, and data rate, respectively. All the aforementioned parameters and their values used for link calculation are listed in Table 5. The link margins for the stomach, and large and small intestines are plotted in Fig. 13. It is observed that in various implanted scenarios, the proposed endoscopic antenna can reliably transmit data over a distance of more than 7 m at 40 dB margins for both frequencies.

TABLE 5. Important parameters considered for link budget analysis.

Parameters	Variables	Value
Resonance frequency	f_o (MHz)	402 / 915
Noise power density	N_o (dB/Hz)	-203.93
Transmitter power	P_{Tx} (dBm)	-4
Polarization mismatch loss	P_L (dB)	1
Temperature	T_o (Kelvin)	273
Free space path loss	L_f (dB)	Distance dependent
Transmitter antenna gain	G_{Tx} (dBi)	Scenario dependent
Receiver antenna gain	G_{Rx} (dBi)	2
Boltzmann Constant	K	1.38×10^{-23}
Available power	A_P (dB)	Distance dependent
Bit rate	B_r (Mbps)	1
Required power	R_P (dB)	-134.64
Margin	A_p -R_p (dB)	Fig. 13

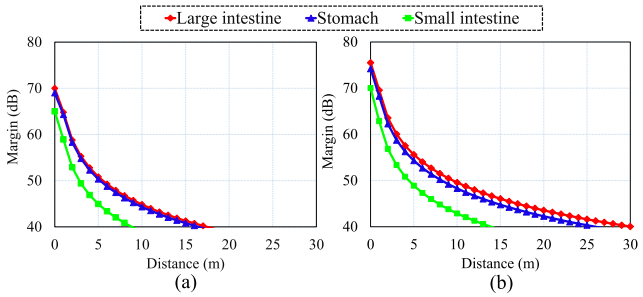

FIGURE 13. Link budget analysis at 1 Mbps in different implanted organs. (a) 402 MHz. (b) 915 MHz.

V. CONCLUSION

A multi-band ingestible antenna encompassing five bands (i.e., the MedRadio, midfield, and three ISM bands) was proposed for multi-tasking. The prominent radiation characteristics with satisfactory gains in the aforementioned bands and a wider bandwidth in the MedRadio band were achieved with a more miniaturized size of 48.98 mm^3 (conformal form) compared to state-of-the-art implantable antennas. The shorting pin and open-ended slots in the patch and ground were found to be helpful for miniaturization, frequency tuning, bandwidth enhancement, and impedance matching. Moreover, the designed antenna was encapsulated with batteries and related dummy circuitry to constitute the capsule architecture. The link budget and SAR analysis were conducted to ensure the reliability of the wireless link and user safety, respectively. The simulated parameters of the fabricated 3D capsule in various scenarios were experimentally validated via measurements conducted using minced pork. The proposed conformal antenna encapsulated in a 3D capsule can be employed beneficially for multitasking (i.e., telemetry, power saving, and WPT) owing to its conformal structure, omni-directional patterns, multi-band operation, and wider bandwidth in the MedRadio band.

REFERENCES

[1] M. Suzan Miah, A. Noor khan, C. Icheln, K. Haneda, and K.-I. Takizawa, "Antenna systems for wireless capsule endoscope: Design, analysis and experimental validation," Apr. 2018, *arXiv:1804.01577*. [Online]. Available: http://arxiv.org/abs/1804.01577

[2] Z. Bao, Y.-X. Guo, and R. Mittra, "Conformal capsule antenna with reconfigurable radiation pattern for robust communications," *IEEE Trans. Antennas Propag.*, vol. 66, no. 7, pp. 3354–3365, Jul. 2018.

[3] D. Nikolayev, M. Zhadobov, L. Le Coq, P. Karban, and R. Sauleau, "Robust ultraminiature capsule antenna for ingestible and implantable applications," *IEEE Trans. Antennas Propag.*, vol. 65, no. 11, pp. 6107–6119, Nov. 2017.

[4] S. Heun Lee, J. Lee, Y. Joong Yoon, S. Park, C. Cheon, K. Kim, and S. Nam, "A wideband spiral antenna for ingestible capsule endoscope systems: Experimental results in a human phantom and a pig," *IEEE Trans. Biomed. Eng.*, vol. 58, no. 6, pp. 1734–1741, Jun. 2011.

[5] S. Yun, K. Kim, and S. Nam, "Outer-wall loop antenna for ultrawideband capsule endoscope system," *IEEE Antennas Wireless Propag. Lett.*, vol. 9, pp. 1135–1138, 2010.

[6] K. Zhang, C. Liu, X. Liu, H. Guo, and X. Yang, "Miniaturized circularly polarized implantable antenna for ISM-band biomedical devices," *Int. J. Antennas Propag.*, vol. 2017, pp. 1–9, Mar. 2017.

[7] C. Liu, Y.-X. Guo, and S. Xiao, "Circularly polarized helical antenna for ISM-band ingestible capsule endoscope systems," *IEEE Trans. Antennas Propag.*, vol. 62, no. 12, pp. 6027–6039, Dec. 2014.

[8] Z. Bao, Y.-X. Guo, and R. Mittra, "Single-layer dual-/tri-band inverted-F antennas for conformal capsule type of applications," *IEEE Trans. Antennas Propag.*, vol. 65, no. 12, pp. 7257–7265, Dec. 2017.

[9] F. Faisal and H. Yoo, "A miniaturized novel-shape dual-band antenna for implantable applications," *IEEE Trans. Antennas Propag.*, vol. 67, no. 2, pp. 774–783, Feb. 2019.

[10] Y. Liu, Y. Chen, H. Lin, and F. H. Juwono, "A novel differentially fed compact dual-band implantable antenna for biotelemetry applications," *IEEE Antennas Wireless Propag. Lett.*, vol. 15, pp. 1791–1794, 2016.

[11] S. A. A. Shah and H. Yoo, "Scalp-implantable antenna systems for intracranial pressure monitoring," *IEEE Trans. Antennas Propag.*, vol. 66, no. 4, pp. 2170–2173, Apr. 2018.

[12] M. Zada and H. Yoo, "A miniaturized triple-band implantable antenna system for bio-telemetry applications," *IEEE Trans. Antennas Propag.*, vol. 66, no. 12, pp. 7378–7382, Dec. 2018.

[13] A. Basir, M. Zada, Y. Cho, and H. Yoo, "A dual-circular-polarized endoscopic antenna with wideband characteristics and wireless biotelemetric link characterization," *IEEE Trans. Antennas Propag.*, early access, Jun. 9, 2020, doi: 10.1109/TAP.2020.2998874.

[14] I. Gani and H. Yoo, "Multi-band antenna system for skin implant," *IEEE Microw. Wireless Compon. Lett.*, vol. 26, no. 4, pp. 294–296, Apr. 2016.
[15] F. Faisal, M. Zada, A. Ejaz, Y. Amin, S. Ullah, and H. Yoo, "A miniaturized dual-band implantable antenna system for medical applications," *IEEE Trans. Antennas Propag.*, vol. 68, no. 2, pp. 1161–1165, Feb. 2020.
[16] H.-Y. Lin, M. Takahashi, K. Saito, and K. Ito, "Performance of implantable folded dipole antenna for in-body wireless communication," *IEEE Trans. Antennas Propag.*, vol. 61, no. 3, pp. 1363–1370, Mar. 2013.
[17] J.-Z. Bao, S.-T. Lu, and W. D. Hurt, "Complex dielectric measurements and analysis of brain tissues in the radio and microwave frequencies," *IEEE Trans. Microw. Theory Techn.*, vol. 45, no. 10, pp. 1730–1741, Oct. 1997.
[18] A. Kiourti, M. Christopoulou, S. Koulouridis, and K. S. Nikita, "Design of a novel miniaturized implantable PIFA for biomedical telemetry," in *Proc. Int. Conf. Wireless Mobile Commun. Healthcare*. Berlin, Germany: Springer, 2010, pp. 127–134.
[19] X. Cheng, D. E. Senior, C. Kim, and Y.-K. Yoon, "A compact omni-directional self-packaged patch antenna with complementary split-ring resonator loading for wireless endoscope applications," *IEEE Antennas Wireless Propag. Lett.*, vol. 10, pp. 1532–1535, 2011.
[20] M. Zada, I. A. Shah, and H. Yoo, "Metamaterial-loaded compact high-gain dual-band circularly polarized implantable antenna system for multiple biomedical applications," *IEEE Trans. Antennas Propag.*, vol. 68, no. 2, pp. 1140–1144, Feb. 2020.
[21] M. Zada and H. Yoo, "Miniaturized dual band antennas for intra-oral tongue drive system in the ISM bands 433 MHz and 915 MHz: Design, safety, and link budget considerations," *IEEE Trans. Antennas Propag.*, vol. 67, no. 9, pp. 5843–5852, Sep. 2019.

MUHAMMAD YOUSAF received the B.Sc. degree in electronics engineering from the University of Engineering and Technology (UET) Taxila, Pakistan, in 2014, and the M.Sc. degree in electrical engineering from COMSATS University Islamabad, in 2017. He is currently a Ph.D. Research Scholar with UET Taxila, where he is working under ACTSENA Research Group focused on implantable antennas and systems, RF coils, wireless power transfer, image processing, and passive chipless RFID tags.

ISMAIL BEN MABROUK (Senior Member, IEEE) received the B.A.Sc. and M.A.Sc. degrees in electrical engineering from the University of Lille, Lille, France, in 2006 and 2007, respectively, and the Ph.D. degree in electrical engineering from the University of Quebec, Canada, in 2012. From 2007 to 2009, he was with Huawei Technologies, Paris, France. He joined the Wireless Devices and Systems (WiDeS) Group, University of Southern California, Los Angeles, CA, USA, in 2012. He is currently an Assistant Professor with Al Ain University of Science and Technology, Abu Dhabi, United Arab Emirates. His research interests include antenna design at the millimeter-wave and THz frequencies, propagation studies for multiple-input and multiple-output (MIMO) systems, deep learning, and wireless body area network for medical applications. He was a recipient of the Abu Dhabi Award for Research Excellence (AARE) – 2018.

FAROOQ FAISAL was born in Buner, Pakistan, in 1993. He received the B.Sc. degree in telecommunication engineering from the University of Engineering and Technology, Peshawar, Pakistan, in 2016, and the M.Sc. degree in telecommunication engineering from University of Engineering and Technology, Taxila, Pakistan, in 2019. He is currently pursuing the Ph.D. degree in electrical engineering with the University of Quebec, Canada. His current research interests include implantable antennas and devices, wireless power transfer, millimetre-wave antennas, wearable antennas for remote underground mine monitoring systems, frequency selective surfaces, EBGs, and portable microwave hybrid imaging based scanners.

MUHAMMAD ZADA received the B.Sc. degree in telecommunication engineering from the University of Engineering and Technology, Peshawar, Pakistan, in 2015. He is currently pursuing the M.S./Ph.D. degrees in biomedical engineering with Hanyang University, Seoul, South Korea. He has published over 11 papers in high-quality journals and conferences proceedings in the field of telecommunications and biomedical engineering. His current research interests include implantable antennas and devices, intra-oral tongue drive systems, wireless power transfer, millimeter-wave antennas, wearable sensors and antennas, MRI and RF coils, microwave breast cancer detection, frequency-selective surfaces, and EBGs. He received the Best Student Paper Competition 2018 by the Korean Institute of Electromagnetic Engineering & Science (KIEES). He is serving as a Reviewer for the IEEE TRANSACTIONS, RFCAD, and Elsevier journals.

ZUBAIR BASHIR received the B.Sc. degree in telecommunication engineering from the University of Engineering and Technology Taxila, Pakistan, in 2019, where he is currently pursuing the M.Sc. degree with the Telecommunication Engineering Department. He joined the ACTSENA Research Group, University of Engineering and Technology Taxila. His research interests include implantable antennas, meta-material, multiple-input and multiple-output (MIMO) systems, and reconfigurable antennas.

ADEEL AKRAM received the B.S. degree in electrical engineering from the University of Engineering and Technology Lahore, Pakistan, in 1995, the M.S. degree in computer engineering from National University of Sciences and Technology (NUST), Pakistan, in 2000, and the Ph.D. in electrical engineering from University of Engineering and Technology Taxila, Pakistan, in 2007. He is currently the Dean and a Professor with the Telecommunication Engineering Department, University of Engineering and Technology Taxila, Pakistan. He is leading a 5G Wireless Communication Group, UET Taxila. His research interests include microwave and communication systems.

MOURAD NEDIL (Senior Member, IEEE) received the Dipl.Ing. degree from the University of Algiers (USTHB), Algiers, Algeria, in 1996, the D.E.A. (M.S.) degree from the University of Marne la Vallée, Marne la Vallée, France, in 2000, and the Ph.D. degree from the Institut National de la Recherche Scientifique (INRS-EMT), Université de Québec, Montréal, QC, Canada, in April 2006.

From 2006 to 2008, he completed a Postdoctoral Fellowship with the RF Communications Systems Group, INRS-EMT. He joined the Engineering School Department, University of Quebec at abitibi-Témiscamingue, Val d'Or, QC, in June 2008, where he is currently a Full Professor. His research interests include antennas, MIMO radio-wave propagation, and microwave devices.

HYOUNGSUK YOO (Senior Member, IEEE) received the B.Sc. degree in electrical engineering from Kyungpook National University, Daegu, South Korea, in 2003, and the M.Sc. and Ph.D. degrees in electrical engineering from the University of Minnesota, Minneapolis, MN, USA, in 2006 and 2009, respectively.

He joined the Center for Magnetic Resonance Research, University of Minnesota, as a Postdoctoral Associate, in 2009. He joined the Cardiac Rhythm Disease Management, Medtronic, Minneapolis, as a Senior MRI Scientist, in 2010. From 2011 to 2018, he was an Associate Professor with the Department of Biomedical Engineering, School of Electrical Engineering, University of Ulsan, Ulsan, South Korea. Since 2017, he has been the CEO of E2MR, Seoul, South Korea, a startup company. Since 2018, he has been an Associate Professor with the Department of Biomedical Engineering, Hanyang University, Seoul. His current research interests include electromagnetic theory, numerical methods in electromagnetics, metamaterials, antennas, implantable devices, and magnetic resonance imaging in high-magnetic field systems.